Desalination and Water Treatment
www.deswater.com

doi: 10.5004/dwt.2018.23198

129 (2018) 309–318
October

Study on the fabrication and properties of polyphenylene sulfide (PPS) membrane and its application in VMD

Tingting Fan, Zhenhuan Li*, Bowen Cheng*

State Key Laboratory of Separation Membranes and Membrane Processes, Department of Material Science and Engineering, Tianjin Polytechnic University, No. 399 West Binshui Road, Xi Qing District, Tianjin 300387, China, Tel. +86 022 83955358; email: Zhenhuanli1975@aliyun.com (Z. Li), Tel. +86 13802163663; email: bowen15@tjpu.edu.cn (B. Cheng), Tel. +86 15802246362; email: 15802246362@163.com (T. Fan)

Received 7 August 2017; Accepted 2 May 2018

ABSTRACT

Polyphenylene sulfide (PPS) membranes were fabricated via a thermally induced phase separation method using mixed diluent of epsilon-caprolactam (CPL) and diphenyl sulfone (DPS). The effect of changing the CPL/DPS weight ratio on the structure and properties of prepared PPS membranes were investigated. The morphologies and performances of obtained PPS membranes were characterized by scanning electron microscopy, static water contact angles, mechanical strength, porosity, permeability and salt rejection rate. The characterized results showed that the morphologies of PPS membrane changed from cellular, bi-continuous to spherulitic structure with the increase of CPL/DPS mass ratio. PPS membranes exhibited the excellent stability and high salt rejection ratio in VMD experiments. The largest permeate flux stabilized at 10.63 L/(m^2·h^1) and the highest salt rejection remained above 98.9% after operating for 10 h.

Keywords: Polyphenylene sulfide (PPS); Flat-sheet membranes; Thermally induced phase separation; Properties; Membrane distillation

1. Introduction

Nowadays, water shortage and purification of sewage are major problems around the world. Membrane technology is an energy saving and efficient wastewater treatment. Membrane distillation (MD) is carried out by means of hot steam driven by hydrophobic microporous membranes. It is a low cost and energy saving membrane separation technology [1–3].

There are four types of MD technologies: direct contact MD, sweep gas MD, air gap MD and vacuum MD (VMD) [4]. Because of the low energy consumption, mild operating conditions and high separation efficiency, VMD has a wide range of potential applications in seawater desalination, removal of heavy metals and volatile organic compounds, wastewater treatment and various separation processes [5–8].

Intrinsic hydrophobic material, such as polypropylene (PP), polytetrafluoroethylene (PTFE), polyvinylidenefluoride (PVDF), is commonly used in MD process [9–13]. However, it is not possible to use PVDF and PP for some MD processes in harsh water environments (high temperature, containing acid or alkali and organic solvents). Thus, it requires a kind of membrane material with excellent performance used for this MD process [14]. Polyphenylene sulfide (PPS) is a semi-crystalline thermoplastic with high melting temperature (285°C–296°C). Most importantly, PPS has excellent solvent resistance, and nearly no solvent can dissolve it below 200°C [15]. Compared with these three membranes, PPS membrane had superior performance against strong acid, strong alkaline and polar solvent, and it possessed the perfect thermal stability [16]. Therefore, PPS is expected to be a promising membrane separation material in the future [17].

* Corresponding authors.

Presented at 2017 Qingdao International Water Congress, June 27–30, 2017, Qingdao, China.

However, the preparation of PPS membrane by the solution phase conversion method is not feasible because it is difficult to find a suitable diluent to dissolve the PPS at a low temperature. PPS membranes can be prepared by thermally induced phase separation (TIPS) [16]. TIPS was first introduced by Castro and was used by several people for the preparation of microporous polymeric membranes. This method has been applied to various crystalline polymers, such as PP [18,19], PE [20,21], PVDF [22–24], polyacrylonitrile (PAN) [25,26] and poly(ethylene-co-vinyl alcohol) (EVOH) [27,28].

TIPS is one of the main techniques for the preparation of polymeric porous membranes by controlling phase separation [29]. TIPS can be divided into two processes: liquid–liquid (L–L) phase separation and solid–liquid (S–L) phase separation [30]. In the TIPS process, a polymer is dissolved in a diluent at a high temperature with the cooling of the solution. The theoretical phase diagrams in TIPS process have been described in many literatures [31,32], as shown in Fig. 1. When the cooling temperature reaches a bimodal curve, L–L separation is induced. As for L–L separation, two mechanisms must be considered: nucleation growth (NG) and spinodal decomposition (SD) [33]. The NG mechanism occurs in a metastable region in the phase diagram between spinodal and binodal curves, while SD is in an unstable region under spinodal curve. Thus, membranes formed by SD or NG mechanisms lead to different porosity morphology and polymer crystallization structure. S–L separation occurs when the cooling temperature reaches the crystallization curves of the polymer. Then the polymer crystallizes and the polymer diluent structure is immobilized. The dilution was extracted with a volatile solvent to form a microporous polymer membrane [34].

The location of the binodal curve is determined by the compatibility of the system, which is quantified as the interaction parameter between polymer and diluent. When L–L phase separation precedes S–L phase separation (Approach 1 in Fig. 1), cellular or bi-continuous structures are obtained. Otherw (Approach 2 in Fig. 1), spherulitic structures are formed by S–L phase separation. When the polymer–diluent interaction is weak (Fig. 1(a)), part of binodal curve is above the crystallization curve and the system undergoes L–L phase separation with subsequent polymer crystallization. When the polymer–diluent interaction is strong (Fig. 1(b)), the binodal curve is lower than the crystallization curve and the system undergoes S–L phase separation in the form of polymer crystallization. The diluent plays an important role in controlling the phase separation mechanism and determines the morphology of membrane.

Up to now, a few studies have been reported on fabrication of PPS microporous membrane via TIPS method [17,35]. In previous studies, PPS membranes with the monotonous structure were prepared by PPS/single diluent systems. Ding et al. [35] used diphenyl sulfone (DPS) or diphenyl ketone as the single diluent to prepare porous PPS membranes. Zheng et al. [17] used six types of solvents to prepare PPS membranes by PPS–single diluent systems, and the formation of various PPS membrane structures were attributed to the different S–L or L–L phase separation mechanism. These prepared PPS membranes had poor permeability and mechanical properties and could not meet the requirements of industrial applications. Recently, some microporous polymeric membranes prepared by TIPS method by using a diluent mixture showed good results in controlling the membrane structure. The structures of membranes based on PVDF [34,36], PE [21] and ECTFE [37] have been systematically controlled by using diluent mixture to control the polymer–diluent interaction.

In this work, PPS membranes with cellular-like, bi-continuous and spherulitic structures were prepared via TIPS process using epsilon-caprolactam (CPL) and DPS as mixed diluent. The main aim of this work was to interpret the forming mechanism of membrane structure by varying diluent composition. Furthermore, the effects of CPL content on the PPS membranes' performances in terms of hydrophobicity, permeability and mechanical strength were also investigated. Subsequently, these PPS membranes were tested in VMD.

2. Experimental section

2.1. Materials

PPS resin, which used in this study, was supplied by Tianjin Petrochemical Co., Ltd., China Petroleum & Chemical

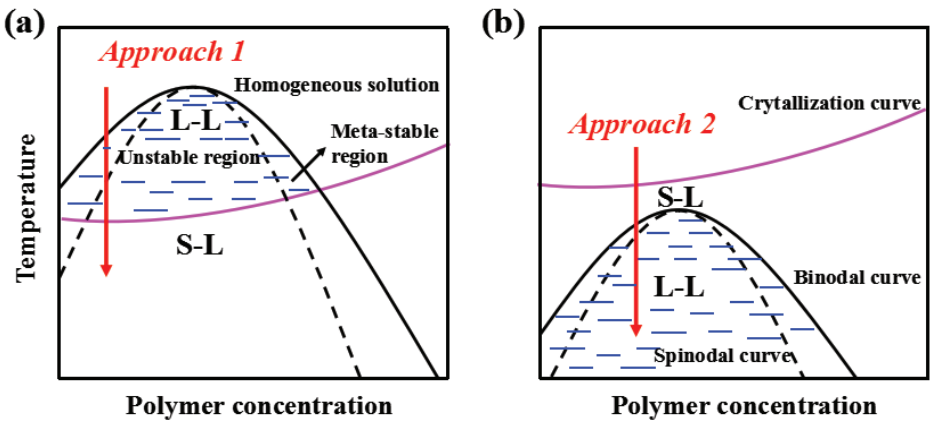

Fig. 1. Different approaches for L–L and S–L phase separation occurring in different systems: (a) system with weak interaction and (b) system with strong interaction.

Corporation (SINOPEC, Tianjin) and it was dried at 120°C for 12 h before use. DPS was purchased from Aladdin Biochemical Technology Co., Ltd (Aladdin, Shanghai). CPL was provided by Tianjin Guangfu Fine Chemical Institute (Tianjin, China). All the chemicals were used without further purification.

2.2. Preparation of PPS flat sheet membranes

PPS flat microporous membranes were prepared via TIPS. A PPS solution mixed with proper amounts of DPS and CPL (diluent) was stirred at 265°C for 15 min under nitrogen atmosphere in a three-neck flask equipped with a mechanical stirrer and a thermometer. After degassing the air bubbles, the casting solution was quickly poured onto the surface of stainless steel plate (Fig. 2) which was preheated to 265°C on a heating plate (Shanghai Bangxi Instruments Technology Co., China), and it was quickly scraped with a casting bar (500 μm). After that, the casting solution together with the plate was immediately immersed into a coagulation bath (tap water at 25°C) to solidify the sample. The diluent in the wet membrane was extracted by being immersed in ethanol for 24 h and pure water for 24 h. The final membranes were freeze-dried using a FD-1D-80 freeze dryer (Hanuo Instruments Co., Shanghai, China). Composition and preparation conditions of each membrane are listed in Table 1.

2.3. Characterization

2.3.1. Differential scanning calorimetry

The crystallization temperature of PPS membranes was characterized by differential scanning calorimetry (DSC 200 F3, Netzsch, Germany). Under the protection of N_2, the solid PPS/diluent sample was melted to 270°C at the rate of 10°C/min and then cooled to 25°C at the rate of 10°C/min. During the cooling process, the temperature of the exothermic peak was regarded as crystallization temperature.

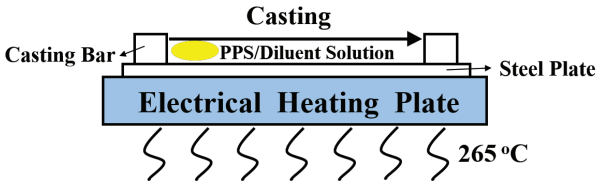

Fig. 2. Schematic of the PPS membrane casting device.

Table 1
Preparation conditions of PPS membranes

Samples	PPS concentration (wt%)	CPL/DPS weight ratio	Cooling water bath (°C)
M-c20	24	20:80	25
M-c24	24	24:76	25
M-c28	24	28:72	25
M-c32	24	32:68	25
M-c50	24	50:50	25
M-c100	24	100:0	25

2.3.2. Membrane morphologies

The morphology of the cross-section and top surface of the PPS flat-sheet membranes were characterized by field-emission scanning electron microscopy (FESEM, Hitachi S-4800, Hitachi, Japan) with an accelerating voltage of 10 kV. Membrane samples were frozen and fractured in liquid nitrogen. Then all samples were coated in gold.

2.3.3. Contact angle measurements

The water contact angle (WCA) of the prepared PPS membrane was measured by using an optical contact angle measuring instrument (model JYSP-180, Jinshengxin Inspection Instrument Co., Ltd., Beijing, China) at room temperature. A 2 μL of water drop was placed on the surface of PPS flat-sheet membranes and the projected drop image was analyzed to determine the static contact angle. Five different spots for each sample were measured and the average value was reported.

2.3.4. Porosity

The porosity of the PPS membrane was determined by the gravimetric method [38], which calculated the weight of liquid immersed in the membrane pores. Due to the hydrophobicity of PPS, *n*-butyl alcohol was used as the wetting liquid. The membrane samples were immersed in the *n*-butyl alcohol for at least 24 h and weighed immediately after removing the *n*-butyl alcohol of the outer membrane surface with a filter paper. The porosity (ε) was calculated by Eq. (1):

$$\mu = \frac{w_2 - w_1}{A \times d \times \rho} \times 100(\%) \quad (1)$$

where w_2 is the weight of the membrane wetted by *n*-butyl alcohol (g), w_1 is the weight of the dry membrane (g), d is the average thickness of the membrane (cm), ρ is the density of *n*-butyl alcohol (ρ = 0.811 g/mL), and A is the area of the PPS membrane (cm^2).

2.3.5. Mechanical strength

The tensile strength and breaking elongation of the prepared PPS membranes were measured by an YG-061-1500 tensile tester at room temperature. Each membrane sample was cut into 5 mm (width) × 25 mm (length) test strips and the tensile rate was 10 mm/min. Each specimen was tested at least five times.

2.3.6. Permeability tests

Pure water flux (PWF) was measured by a self-made cross-flow filtration experimental device. The PPS membrane was pre-pressurized with distilled water at 0.2 MPa for 30 min and then the pressure was adjusted to operation pressure of 0.1 MPa. The PWF was determined by the following Eq. (2):

$$J = \frac{V}{A \times t} \quad (2)$$

where J is the PWF ($L \cdot m^{-2} \cdot h^{-1}$), V is the total permeation (L), A is the effective membrane area (m^2) and t is the permeation time (h).

Nitrogen flux of dry flat membranes was calculated by the following equation (Eq. (3)), and the permeate flow rate was measured at 0.01 MPa:

$$J = \frac{L}{A} \tag{3}$$

where J is the nitrogen flux ($m^3 \cdot m^{-2} \cdot h^{-1}$), L is the nitrogen flow ($m^3 \cdot h^{-1}$) and A is the effective membrane area (m^2).

2.3.7. Liquid entry pressure

Liquid entry pressures (LEPs) of the dry PPS membranes were determined using a laboratory device (Fig. 3) at room temperature. Increased the pressure slowly until the mutation of the conductivity meter, this mutation pressure was considered as the LEP point. The average value of three tests is reported.

2.3.8. Membrane distillation experiments

The performance of the PPS membranes in harsh water desalination was tested with VMD. Fig. 4 shows a setup schematically for the desalination experiment. The hot and circulating salt solution (80°C, 3.5 wt % NaCl) was contacted to the membranes in one side and a vacuum pump (the vacuum pressure is 0.085 MPa) was connected to its other side. The permeate vapor was condensed into liquid water through a condenser and collected as the product. The conductivity of the feed solution and the permeate water was measured by a conductivity meter (FE30K, Mettler Toledo, China). The salt rejection R was calculated by Eq. (4) as follows:

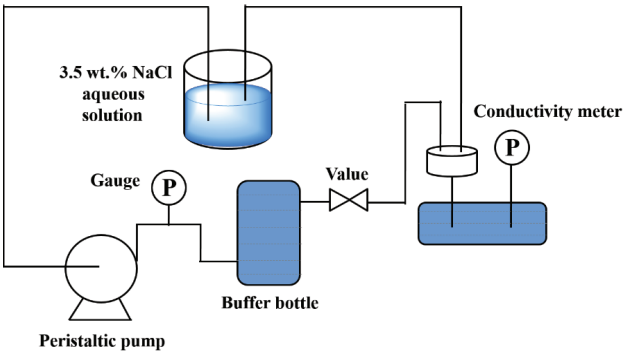

Fig. 3. LEP of the PPS membrane testing device.

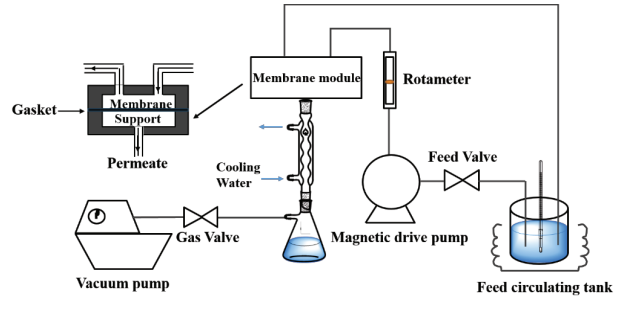

Fig. 4. Schematic diagram of the VMD experiments.

$$R = 1 - \frac{C_p}{C_f} \tag{4}$$

where C_p and C_f were the conductivity of the permeate water and feed solution, respectively.

3. Results and discussion

3.1. Phase diagram

The compatibility of polymer and diluents directly reflects the thermodynamic properties such as the binodal line and crystallization temperature [39]. Membrane morphology was affected by the different phase separation mechanism, which could be seen from the phase diagram. When L–L phase separation occurred before polymer crystallization, a cellular or bi-continuous structure could be observed [40]. On the contrary, in the case of S–L phase separation, only the spherical membrane structure could be obtained, unless this structure could be modulated by acting on polymer concentration, cooling rate and polymer/diluent interaction [34]. The binary phase diagram for the PPS–CPL, PPS–DPS system is shown in Figs. 5 and 6, respectively. The monotectic point (ϕ_m) of PPS–DPS was between 30% and 40%, the L–L region was located left of ϕ_m and the S–L region was located below ϕ_m. However, the curve of crystallization points was higher than curve of cloud-points (the temperature of the liquid–liquid phase separation of the system) in the PPS–CPL system, which showed that the PPS–CPL system exhibited only a solid–liquid (S–L) phase separation region without liquid–liquid (L–L) phase separation region. As a result, DPS had a lower compatibility with PPS than CPL [39].

The phase diagram of PPS/CPL/DPS ternary systems with different CPL/DPS mass ratios at the PPS concentration of 24 wt % is shown in Fig. 7. It could be seen,

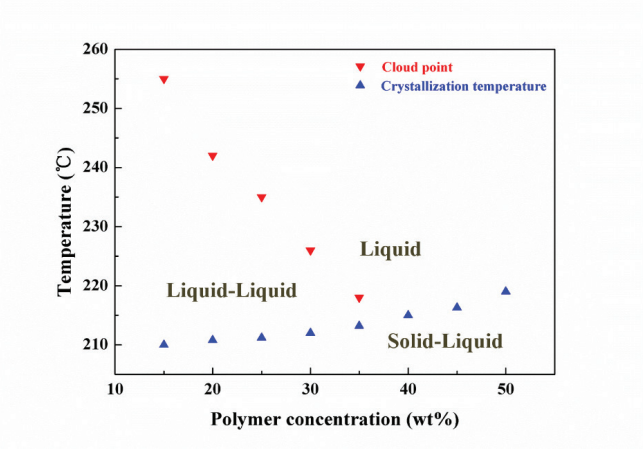

Fig. 5. Binary equilibrium phase diagram for the PPS–DPS system.

when the CPL/DPS weight ratio in mixed diluent reached 35 wt %/65 wt %, L–L phase separation was no longer observed, and only the polymer crystallization process existed. But the PPS/DPS system was L–L phase separation when the PPS concentration was 24 wt %. It was clear that the increase of CPL/DPS mass ratio promoted the occurrence of S–L phase separation. In other words, it enhanced the compatibility between polymer and diluent. When the compatibility between polymer and diluent was enhanced, the L–L phase separation shifted below the S–L phase [23]. Thus, the L–L phase separation occurred before the polymer crystallization owing to the poor compatibility between polymer and diluent. With the further improvement of compatibility, no L–L phase separation happened, but only the S–L phase separation [32].

3.2. Morphologies

The effects of CPL/DPS weight ratio on cross-section and top surface structures of PPS membranes in the L–L phase separation were shown in Fig. 8. As the CPL ratio increased in diluent mixture, several different membrane cross-section morphologies were observed. As the CPL/DPS ratio was 20:80, large cellular pores were obtained in M-c20 as shown in Figs. 8(a-1) and (a-2). The structure of cellular pores, which was typical structure of membrane for L–L phase separation system [41]. But these cellular pores were mostly closed pores. As the DPS/CPL ratio increased to 24:76, the membrane M-c24 had a cellular microstructure without larger pores as shown in Figs. 8(b-1) and (b-2). Because the homogeneous mixture was quenched to the room temperature via TIPS process, phase separation directly entered the unstable region and proceeded through SD [45]. As the DPS/CPL ratio increased to 28:72 and 32:68, a bi-continuous structure was obtained and the pores became smaller as shown in Figs. 8(c-1) and (c-2) and Figs. 8(d-1) and (d-2). As shown in Figs. 8(a-3), (b-3), (c3) and (d3), when the weight ratio of DPS/CPL changed from 20:80 to 32:68, the pore numbers of the membrane top surface (air side) were increased significantly. Since the temperature gap between liquid–liquid phase separation temperature and the crystallization temperature of the polymer played an important role in determining the microstructure of the porous membrane [41]. When the cooling condition was the same, the sample with 20 wt /80 wt DPS/CPL had more time for L–L phase separation than that with 32 wt /68 wt DPS/CPL, thus M-c20 had the larger cellular pores. In the S–L separation systems, the cross section of M-d50 and M-d100 entirely presented spherulitic structure and the spherulites grew bigger as the CPL/DPS ratio increased as shown in Figs. 9(e-1) and (e-2) and Figs. 9(f-1) and (f-2). And the top surface pores of M-d50 and M-d100 became smaller and smaller as shown in Figs. 9(e-3) and (f-3). It was because with higher CPL/DPS ratio the compatibility between PPS and diluent was stronger, which prevented the nucleation activity of PPS and led to the formation of few primary nuclei at the beginning of crystallization [34]. In addition, in the L–L phase separation system, since the CPL/DPS ratio increased in diluent mixture, the pore size decreases, but the number of pores increases. As for the S–L phase separation systems (M-c50 and M-c100), both the pore size and number of pores were reduced.

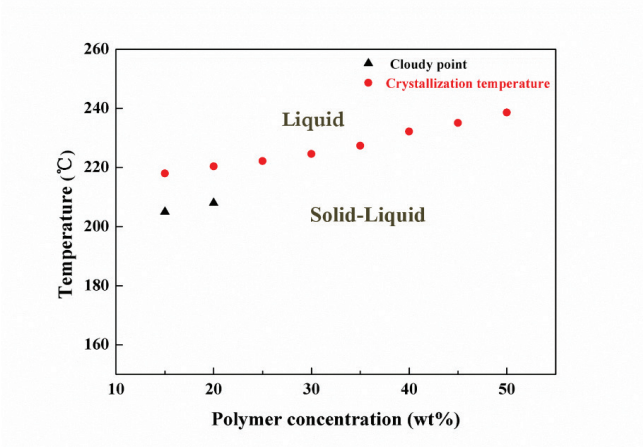

Fig. 6. Binary equilibrium phase diagram for the PPS–CPL system.

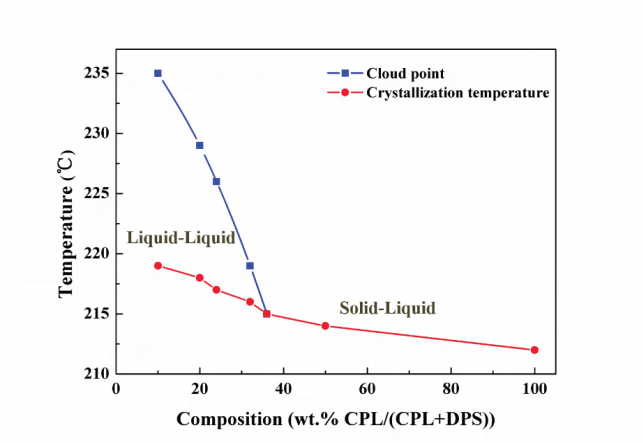

Fig. 7. Phase diagram of PPS/CPL/DPS ternary systems with various weight ratios of CPL/DPS at the PPS concentration of 24 wt %.

3.3. Permeation properties

Effects of CPL/DPS ratio in diluent mixture on the PWF and porosity of PPS membranes were shown in Fig. 10. The results showed that the porosity increased from 53.6% to 68.3% at first then decreased to 47.5% as the CPL ratio increased. And the PWF increased from 31.2 to 75.2 L/m^2·h at first then decreased to 18.6 L/m^2·h as the CPL ratio increased. It could be seen that the porosity and PWF of the M-c32 were much higher than that of the other membranes. This was mainly attributed to the evolution of membrane microstructure changed from cellular, bi-continuous to spherulitic structure with the increase of CPL ratio, which was discussed above. Importantly, the connectivity of bi-continuous structure was better than that of cellular and spherical structure. The change trend of N_2 flux with the increase of CPL/DPS ratio was similar to the trend of porosity. It could be seen that the LEP value decreased at first then increased, the results are shown in Fig. 11.

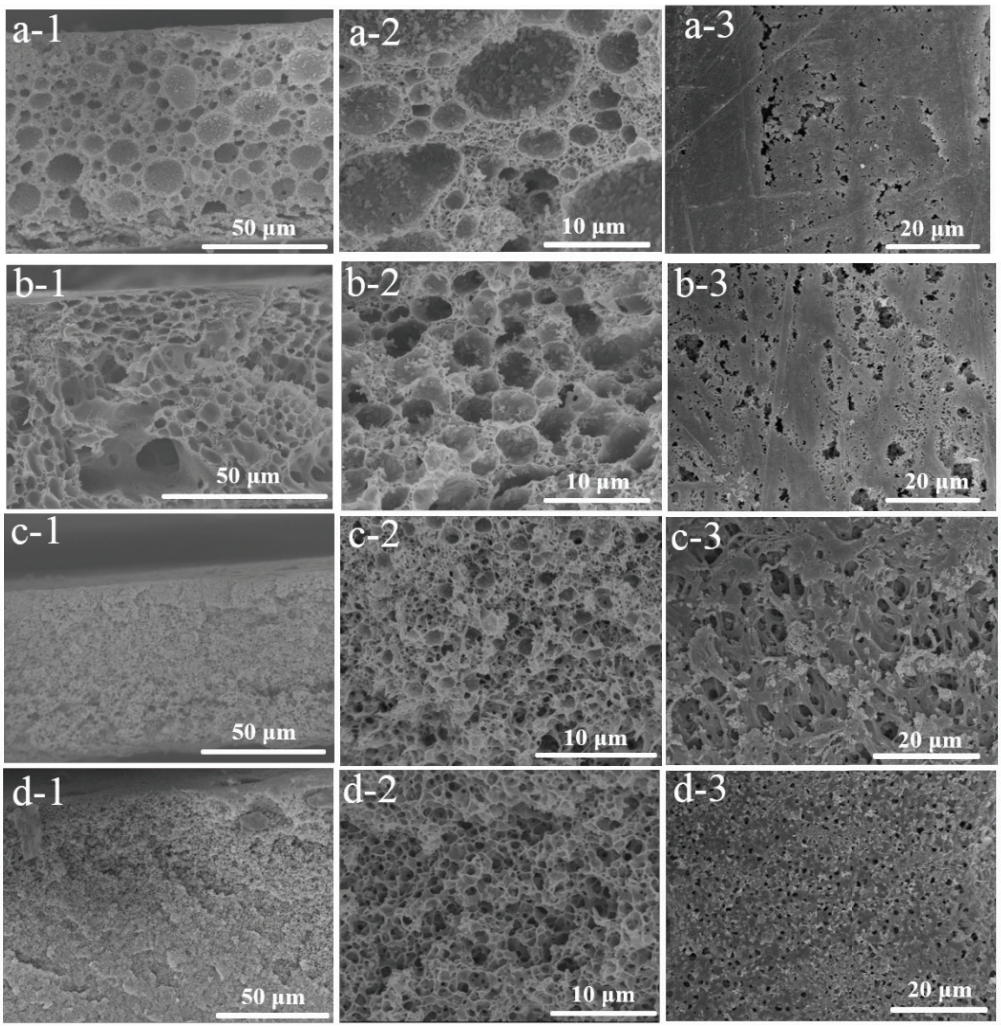

Fig. 8. SEM photographs of PPS membranes prepared via L–L phase separation ((a) M-c20, (b) M-c24, (c) M-c28, (d) M-c32; 1: whole cross section ×700, 2: enlarged cross section ×3,500, 3: the top surface ×1,500).

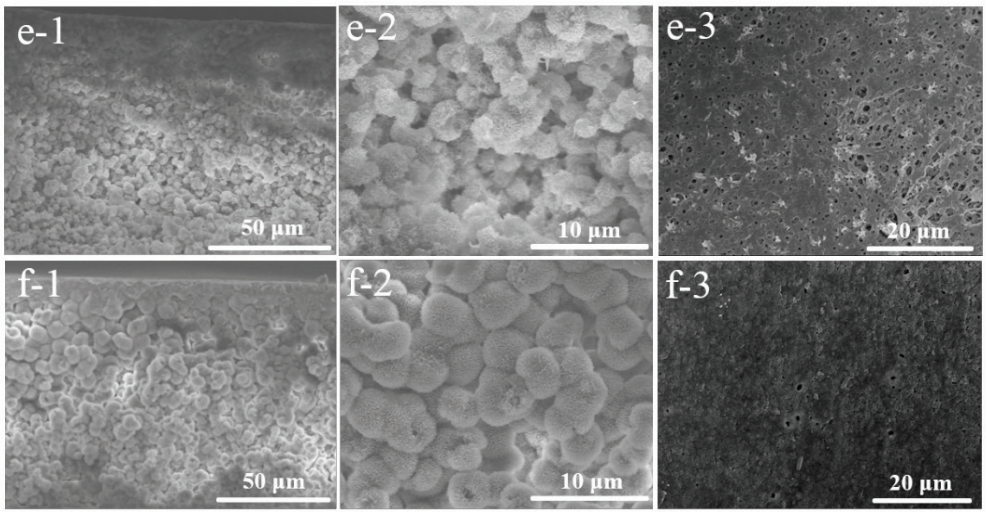

Fig. 9. SEM photographs of PPS membranes prepared via S–L phase separation ((e): M-c50, (f): M-c100; 1: whole cross section ×700, 2: enlarged cross section ×3,500, 3: the top surface ×1,500).

3.4. Wettabilities

Hydrophobicity was the important property for membrane application in VMD [42,43]. Effect of CPL/DPS ratio in diluent mixture on the WCA of PPS membranes is shown in Fig. 12. The results shown that the WCA increased from 92.8° to 121.5° at first then decreased to 88.6° as the CPL/DPS ratio increased from 20 wt/80 wt to 100 wt/0 wt.

3.5. Membrane mechanical properties

The effects of weight ratio of CPL to DPS on elongation-at-break and breaking strength of PPS membranes are shown in Fig. 13. As CPL content increased, the tensile strength decreased significantly from 3.86 to 2.79 MPa at first and then increased to 3.55 MPa, and the breaking elongation decreased significantly from 12.6% to 7.9% at first and then slightly increased from 7.9% to 8.3%. It was well known that the microstructure of membranes played the important roles on the mechanical properties of membranes. And the high membrane porosity would weaken the breaking strength [44]. It was clear that the breaking strength of M-c50 and M-c100 was much higher than M-c32. The main reasons were the surfaces of the membrane M-c50 and M-c100 had a thin layer of low porosity. At the same time, the spherulites grew bigger and more perfectly progressively as the CPL/DPS ratio increased and it contribute to the increase of the mechanical strength.

3.6. Membrane distillation performances

Thicknesses, mean pore sizes and maximum pore sizes of the PPS membrane samples are shown in Table 2. In this work, the PPS membranes prepared via L–L phase separation were suitable for VMD experiments. The low porosity and poor hydrophobicity of the membranes (M-c50, M-c100) prepared via S–L phase separation resulted in they could not be used in membrane distillation. The results of VMD permeate flux and salt rejection are shown in Fig. 14. As shown in Fig. 14, the variation tendency of permeate flux was almost same as the variation of N_2 flux for the membrane samples. The increase of N_2 and permeate fluxes could be attributed to the increase of porosity. It could be seen that the M-c32 had a highest stable permeation flux of 10.63 L/(m^2·h^1) and salt rejection remained above 97.4% after operating for 10 h as shown in Fig. 14(d). And the stable permeate flux of M-c28 reached 8.35 L/(m^2·h^1) and the highest salt rejection remained above 98.9% as shown in Fig. 14(c). The M-c20 had a lowest

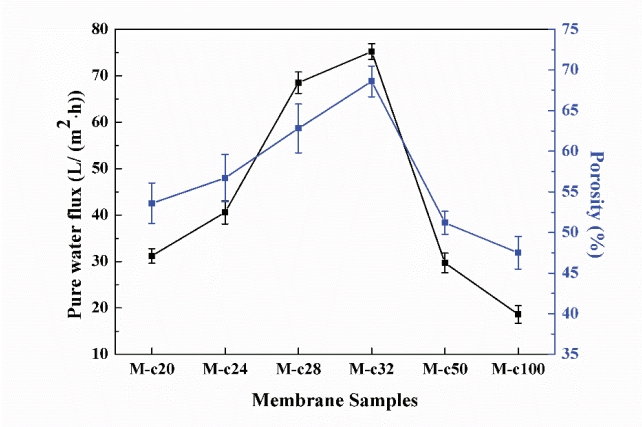

Fig. 10. PWF and porosity of different PPS porous membranes prepared by different diluent mixtures.

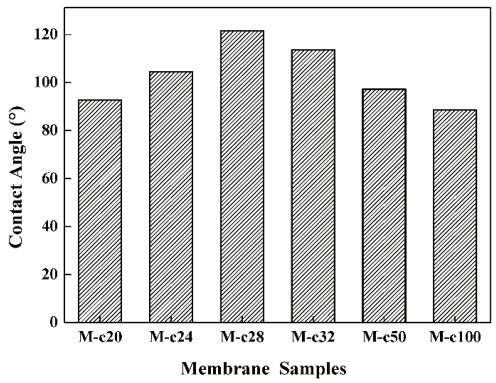

Fig. 12. Water contact angles of different PPS porous membranes prepared by different diluent mixtures.

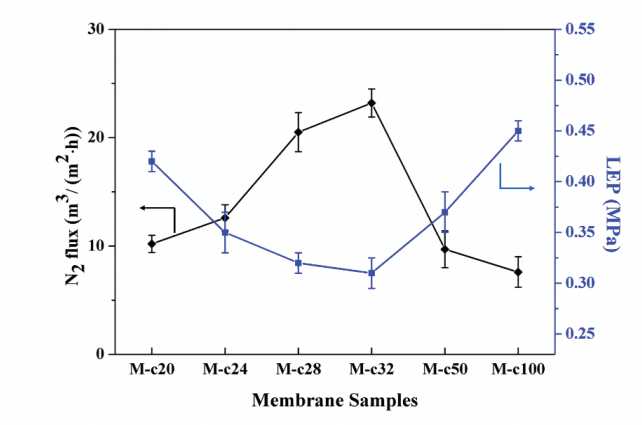

Fig. 11. N_2 flux and LEP of different PPS porous membranes prepared by different diluent mixtures.

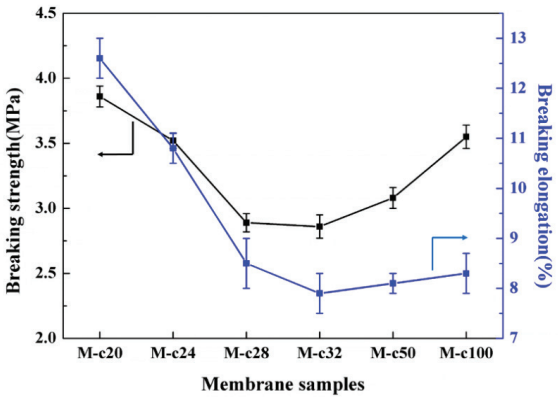

Fig. 13. Mechanical properties of different PPS porous membranes prepared by different diluent mixtures.

Table 2
Thickness, mean pore size and maximum pore size of the PPS membrane samples

Samples	Thickness (μm)	Mean pore size (μm)	Maximum pore size (μm)
M-d20	126.3±2	0.18±0.02	0.22
M-d24	129.5±3	0.21±0.01	0.24
M-d28	125.9±2	0.25±0.02	0.31
M-d32	130.7±4	0.24±0.02	0.29
M-d50	136.5±3	0.22±0.03	0.26
M-d100	138.2±5	0.16±0.01	0.19

permeation flux of 2.37 L/(m^2·h^1) and lowest salt rejection of 81.5%. The hydrophobicity and LEP of the membrane were two important factors that determine the separation properties of MD [37]. Both the LEP and the WCA of M-c28 were larger than other membranes, so the salt rejection of M-c28 was highest. Table 3 listed a performance comparison between this work and other published MD processes [45,46]. It was found that the PPS membranes exhibited a great potential for their use in MD process for seawater treatment.

4. Conclusions

PPS flat sheet membranes were prepared from the ternary systems of PPS/CPL/DPS by TIPS method.

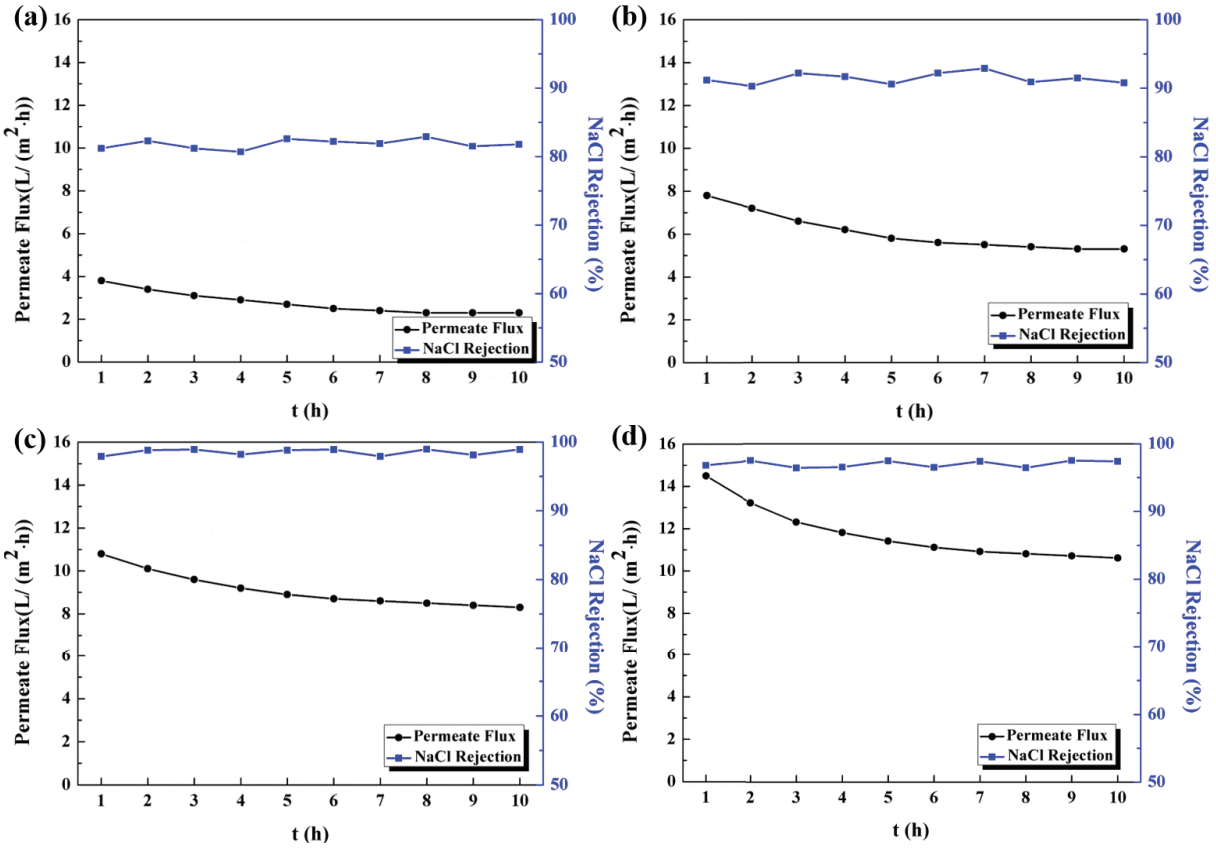

Fig. 14. Permeate flux and salt rejection of PPS membranes (a) M-20, (b) M-d24, (c) M-d28, (d) M-d32 (80°C feed temperature, 0.085 MPa vacuum pressure, 3.5 wt% NaCl).

Table 3
Comparison of the flux obtained in this study with the literature for MD processes

Application	Feed solution	Feed temperature (°C)	NaCl rejection (%)	Driving force Δp (MPa)	Permeation flux (L/(m^2·h))	Membrane code	Refs.
VMD	3.5 wt% NaCl	70	99.9	0.095	2.6	FEP flat-sheet	[45]
VMD	3.5 wt% NaCl	80	97.0	0.015	11.8	PVDF flat-sheet	[46]
VMD	3.5 wt% NaCl	80	98.9	0.085	8.3	PPS flat-sheet (M-c28)	This work
VMD	3.5 wt% NaCl	80	97.4	0.085	10.6	PPS flat-sheet (M-c32)	This work

The phase behaviors of PPS/CPL/DPS system were determined to control systematically L–L phase separation and S–L phase separation by changing the CPL/DPS ratio in diluent mixture. As the weight ratio of CPL increased, the compatibility between PPS and diluents became strong, and the cross section of PPS membrane changed from big cellular to bi-continuous and spherical structure. It was found that the membrane with bi-continuous microstructure possessed higher permeate flux and salt rejection than those of membranes with cellular structure or spherical structure in VMD process. Moreover, the PPS membranes exhibited the excellent stability and high salt rejection ratio in water desalination experiments. Those results show the potential application of this novel type of membrane in the treatment of sewage.

Acknowledgments

The authors are grateful for the financial support from National Natural Science Foundation of China (Nos. 21676202 and 21376177) and Tianjin Natural Science Foundation of China (no. 15JCZDJC7000). This work is also supported by China National Textile and Apparel Council (J201406) and China Petroleum Chemical Co Technology Development Project (208068, 201100, 215038 and 216090).

References

[1] A.M. Alklaibi, N. Lior, Membrane-distillation desalination: status and potential, Desalination, 171 (2005) 111–131.
[2] M.S. El-Bourawi, Z. Ding, R. Ma, M. Khayet, A framework for better understanding membrane distillation separation process, J. Membr. Sci., 285 (2006) 4–29.
[3] E. Curcio, E. Drioli, Membrane distillation and related operations—a review, Sep. Purif. Rev., 34 (2005) 35–86.
[4] M. Qtaishat, T. Matsuura, B. Kruczek, M. Khayet, Heat and mass transfer analysis in direct contact membrane distillation, Desalination, 219 (2008) 272–292.
[5] M. Khayet, Membranes and theoretical modeling of membrane distillation: a review, Adv. Colloid Interface Sci., 164 (2011) 56.
[6] A. Alkhudhiri, N. Darwish, N. Hilal, Membrane distillation: a comprehensive review, Desalination, 287 (2012) 2–18.
[7] P. Wang, T.S. Chung, Recent advances in membrane distillation processes: membrane development, configuration design and application exploring, J. Membr. Sci., 474 (2015) 39–56.
[8] E.R. Abu-Zeid, Y. Zhang, H. Dong, L. Zhang, H.L. Chen, L. Hou, A comprehensive review of vacuum membrane distillation technique, Desalination, 356 (2015) 1–14.
[9] A. Razmjou, E. Arifin, G. Dong, J. Mansouri, V. Chen, Superhydrophobic modification of TiO_2 nanocomposite PVDF membranes for applications in membrane distillation, J. Membr. Sci., 415–416 (2012) 850–863.
[10] J.E. Efome, D. Rana, T. Matsuura, C.Q. Lan, Enhanced performance of PVDF nanocomposite membrane by nanofiber coating: a membrane for sustainable desalination through MD, Water Res., 89 (2016) 39–49.
[11] H. Zhu, H. Wang, F. Wang, Y. Guo, H. Zhang, J. Chen, Preparation and properties of PTFE hollow fiber membranes for desalination through vacuum membrane distillation, J. Membr. Sci., 446 (2013) 145–153.
[12] C.J. Chuang, K.L. Tung, Y.H. Fan, C.D. Ho, J. Huang, Performance evaluation of ePTFE and PVDF flat-sheet module direct contact membrane distillation, Water Sci. Technol., 62 (2010) 347–352.
[13] C.Y. Kuo, H.N. Lin, H.A. Tsai, D.M. Wang, J.Y. Lai, Fabrication of a high hydrophobic PVDF membrane via nonsolvent induced phase separation, Desalination, 233 (2008) 40–47.
[14] K. Chen, C. Xiao, Q. Huang, H. Liu, H. Liu, Y. Wu, Z. Liu, Study on vacuum membrane distillation (VMD) using FEP hollow fiber membrane, Desalination, 375 (2015) 24–32.
[15] W. Tanthapanichakoon, M. Hata, K.H. Nitta, M. Furuuchi, Y. Otani, Mechanical degradation of filter polymer materials: polyphenylene sulfide, Polym. Degrad. Stab., 91 (2006) 2614–2621.
[16] X. Wang, Z. Li, M. Zhang, T. Fan, B. Cheng, Preparation of a polyphenylene sulfide membrane from a ternary polymer/solvent/non-solvent system by thermally induced phase separation, RSC Adv., 7 (2017) 10503–10516.
[17] H. Zheng, S. Zhu, W. Yu, C. Zhou, Comparison of various solvents for poly(phenylene sulfide) microporous membrane preparation via thermally induced phase separation, J. Macromol. Sci. B, 53 (2014) 1477–1496.
[18] B. Luo, Z. Li, J. Zhang, X. Wang, Formation of anisotropic microporous isotactic polypropylene (iPP) membrane via thermally induced phase separation, Desalination, 233 (2008) 19–31.
[19] S.C. Roh, M.J. Park, S.H. Yoo, C.K. Kim, Changes in microporous structure of polyethylene membrane fabricated from PE/PTMG/paraffin ternary mixtures, J. Membr. Sci., 411–412 (2012) 201–210.
[20] H. Matsuyama, H. Okafuji, T. Maki, M. Teramoto, N. Kubota, Preparation of polyethylene hollow fiber membrane via thermally induced phase separation, J. Membr. Sci., 223 (2003) 119–126.
[21] J.P. Mi, C.K. Kim, Fabrication of polyethylene microporous membranes using triethylolpropane tris(2-ethylhexanoate) as a novel diluent by a thermally induced phase separation process, J. Membr. Sci., 449 (2014) 127–135.
[22] Y. Su, C. Chen, Y. Li, J. Li, PVDF membrane formation via thermally induced phase separation, J. Macromol. Sci. A, 44 (2007) 99–104.
[23] G.L. Ji, L.P. Zhu, B.K. Zhu, C.F. Zhang, Y.Y. Xu, Structure formation and characterization of PVDF hollow fiber membrane prepared via TIPS with diluent mixture, J. Membr. Sci., 319 (2008) 264–270.
[24] H.Q. Liang, Q.Y. Wu, L.S. Wan, X.J. Huang, Z.K. Xu, Polar polymer membranes via thermally induced phase separation using a universal crystallizable diluent, J. Membr. Sci., 446 (2013) 482–491.
[25] Q.Y. Wu, L.S. Wan, Z.K. Xu, Structure and performance of polyacrylonitrile membranes prepared via thermally induced phase separation, J. Membr. Sci., 409–410 (2012) 355–364.
[26] Q.Y. Wu, B.T. Liu, M. Li, L.S. Wan, Z.K. Xu, Polyacrylonitrile membranes via thermally induced phase separation: effects of polyethylene glycol with different molecular weights, J. Membr. Sci., 437 (2013) 227–236.
[27] Z. Jing, H. Zhang, H. Wang, Q. Du, Effect of cooling baths on EVOH microporous membrane structures in thermally induced phase separation, J. Membr. Sci., 343 (2009) 104–109.
[28] M. Shang, H. Matsuyama, M. Teramoto, D.R. Lloyd, N. Kubota, Preparation and membrane performance of poly(ethylene-co-vinyl alcohol) hollow fiber membrane via thermally induced phase separation, Polymer, 44 (2003) 7441–7447.
[29] D.R. Lloyd, Materials science of synthetic membranes, ACS, 1985.
[30] D.R. Lloyd, S.S. Kim, K.E. Kinzer, Microporous membrane formation via thermally-induced phase separation. II. Liquid–liquid phase separation, J. Membr. Sci., 52 (1991) 239–261.
[31] P.V.D. Witte, P.J. Dijkstra, J.W.A.V.D. Berg, J. Feijen, Phase separation processes in polymer solutions in relation to membrane formation, J. Membr. Sci., 117 (1996) 1–31.
[32] Z. Song, M. Xing, J. Zhang, B. Li, S. Wang, Determination of phase diagram of a ternary PVDF/γ-BL/DOP system in TIPS process and its application in preparing hollow fiber membranes for membrane distillation, Sep. Purif. Technol., 90 (2012) 221–230.
[33] K.K. Sirkar, D.R. Lloyd, N.M.O. Aiche, New membrane materials and processes for separation, Am. Inst. Chem. Eng., 84 (1988) 261.
[34] G.-L. Ji, B.-K. Zhu, Z.-Y. Cui, C.-F. Zhang, Y.-Y. Xu, PVDF porous matrix with controlled microstructure prepared by TIPS

process as polymer electrolyte for lithium ion battery, Polymer, 48 (2007) 6415–6425.
[35] H. Ding, Q. Zhang, Y. Tian, Y. Shi, B. Liu, Preparation of porous structure in the system of PEEK/PPS/diphenyl ketone via thermally induced phase separation, J. Appl. Polym. Sci., 104 (2007) 1523–1530.
[36] M. Liu, Z. Xu, D. Chen, Y. Wei, Preparation and characterization of microporous PVDF membrane by thermally induced phase separation from a ternary polymer/solvent/non-solvent system, Desal. Wat. Treat., 17 (2010) 183–192.
[37] J. Pan, C. Xiao, Q. Huang, H. Liu, J. Hu, ECTFE porous membranes with conveniently controlled microstructures for vacuum membrane distillation, J. Mater. Chem. A, 3 (2015) 23549–23559.
[38] H. Matsuyama, M. Teramoto, K. Matsui, Y. Kitamura, Preparation of poly(acrylic acid)/poly(vinyl alcohol) membrane for the facilitated transport of CO_2, J. Appl. Polym. Sci., 81 (2001) 936–942.
[39] M. Gu, J. Zhang, X. Wang, H. Tao, L. Ge, Formation of poly(vinylidene fluoride) (PVDF) membranes via thermally induced phase separation, Desalination, 192 (2006) 160–167.
[40] Y. Tang, Y. Lin, W. Ma, T. Ye, Y. Jian, X. Wang, Preparation of microporous PVDF membrane via tips method using binary diluent of DPK and PG, J. Appl. Polym. Sci., 118 (2010) 3518–3523.
[41] H. Matsuyama, S. Berghmans, D.R. Lloyd, Formation of anisotropic membranes via thermally induced phase separation, Polymer, 40 (1999) 2289–2301.
[42] M. Farbod, S. Rezaian, An investigation of super-hydrophilic properties of TiO_2/SnO_2 nano composite thin films, Thin Solid Films, 520 (2012) 1954–1958.
[43] Y.C. Chen, C.C. Tsai, Y.D. Lee, Preparation and properties of silylated PTFE/SiO_2 organic-inorganic hybrids via sol-gel process, J. Polym. Sci. A, 42 (2004) 1789–1807.
[44] Y.-j. Wu, Q.-l. Huang, C.-f. Xiao, K.-k. Chen, X.-f. Li, N.-n. Li, Study on the effects and properties of PVDF/FEP blend porous membrane, Desalination, 353 (2014) 118–124.
[45] K. Chen, C. Xiao, Q. Huang, C. Zhang, Y. Wu, H. Liu, Z. Liu, Study on the fabrication and properties of FEP/SiO_2 hybrid flat-sheet membrane and its application in VMD, Desal. Wat. Treat., 57 (2016) 1–11.
[46] C.l-K. Chiam, R. Sarbatly, Heat transfer in the rectangular cross-flow flatsheet membrane module for vacuum membrane distillation, Chem. Eng. Process., 79 (2014) 23–33.